Front. Earth Sci. 2016, 10(3): 479–486
DOI 10.1007/s11707-016-0561-8

RESEARCH ARTICLE

Satellite remote sensing of the island mass effect on the Sub-Antarctic Kerguelen Plateau, Southern Ocean

Babula JENA (✉)

ESSO-National Centre for Antarctic and Ocean Research, Ministry of Earth Sciences (MoES), Headland Sada, Goa 403804, India

Abstract The presence of the Kerguelen Plateau and surrounding bathymetric features has a strong influence on the persistently eastward flowing Antarctic Circumpolar Current (ACC), resulting in enhancement of surface chlorophyll-a (Chl-*a*) in the downstream section of the plateau along the polar front (PF). The phenomenon is reported in this paper as the island mass effect (IME). Analysis of climatological Chl-*a* datasets from Aqua-Moderate Resolution Imaging Spectroradiometer (Aqua-MODIS) and Sea-viewing Wide Field-of-view Sensor (SeaWiFS) shows distinct bloomy plumes (Chl-$a > 0.5$ mg/m^3) during austral spring-summer spreading as far as ~1800 km offshore up to 98°E along the downstream of the north Kerguelen Plateau (NKP). Similar IME phenomena is apparent over the south Kerguelen Plateau (SKP) with the phytoplankton bloom extending up to 96.7°E, along the southern boundary of ACC. The IME phenomena are pronounced only during austral spring-summer period with the availability of light and sedimentary source of iron from shallow plateau to sea surface that fertilizes the mixed layer. The NKP bloom peaks with a maximum areal extent of 1.315 million km^2 during December, and the SKP bloom peaks during January with a time lag of one month. The blooms exist for at least 4 months of a year and are significant both as the base of regional food web and for regulating the biogeochemical cycle in the Southern Ocean. Even though the surface water above the Kerguelen Plateau is rich in Chl-*a*, an exception of an oligotrophic condition dominated between NKP and SKP due to apparent intrusion of iron limited low phytoplankton regime waters from the Enderby basin through the north-eastward Fawn Trough Current.

Received July 3, 2015; accepted October 7, 2015

E-mail: jena_ocean@yahoo.co.in

Keywords island mass effect, Antarctic Circumpolar Current, Aqua-MODIS, SeaWiFS

1 Introduction

The occurrence of enhanced primary production off an island in the wake of an eddy flow is reported as the island mass effect (IME) (Doty and Oguri, 1956), and the phenomenon can be exhibited to investigate natural iron enrichment for high-nutrient low-chlorophyll (HNLC) systems. Iron (Fe) is essential for marine phytoplankton growth (Sunda, 1989). The Southern Ocean is known as the largest HNLC region of the global ocean (Martin et al., 1990; Minas and Minas, 1992). Earlier mesoscale iron fertilization investigations revealed strong influence of micronutrient iron on phytoplankton biomass and community composition in the Southern Ocean (Boyd et al., 2000; Coale et al., 2004). Direct deposition of micronutrient iron from mineral dust is low into the Southern Ocean (Luo et al., 2003; Zender et al., 2003). There are locations in the vicinity of islands and their down-streams where iron from islands and surrounding shallow plateau enhances phytoplankton biomass owing to IME (Venables and Moore, 2010). This can contribute to productivity and fishery resources in and around islands (Heywood et al., 1990; Signorini et al., 1999), and also for the global CO_2 budget (Heywood et al., 1996). Satellite observations from Coastal Zone Color Scanner (CZCS) and Sea-viewing Wide Field-of-view Sensor (SeaWiFS) data have shown the IME off Madeira Island (Caldeira et al., 2002), Galapagos Islands (Palacios, 2002), and Crozet Archipelago (Bakker et al., 2007). The present work focuses on the scope of satellite remote sensing observations from Aqua-Moderate Resolution Imaging Spectroradiometer (Aqua-MODIS) and SeaWiFS to study the IME phenomena around the Kerguelen Plateau and characterizes the

monthly evolution of phytoplankton blooms during austral spring-summer period.

2 Data analysis and methodology

The Kerguelen Plateau is an extensive submarine topographic high in the Indian Ocean sector of the Southern Ocean bounded by deep ocean basins. Figure 1(a) illustrates the bathymetry of the region mapped using Earth Topography One Arc-Minute Global Relief Model, 2009 (ETOPO1) ice surface version geo-referenced data (21601 by 10801 cells) obtained from www.ngdc.noaa.gov. Northeast shifting of pixel location in ETOPO1 was rectified as the method specified in Jena et al. (2012). The maximum length of the Plateau is approximately 2350 km (restricted between 45°S and 63.5°S latitude) with overall orientation of a Northwest to Southeast trend towards the Antarctic continent. The meridional extent stretches from 61°E to 86°E. The Plateau can be divided into two parts such as the north Kerguelen Plateau (NKP) and the south Kerguelen Plateau (SKP), which is separated by the Fawn Trough (Fig. 1(a)). The FT allows the eastward Antarctic Circumpolar Current (ACC) to flow through the narrow channel. The ACC comprises three major circumpolar fronts: the subantarctic front (SAF), polar front (PF), and southern ACC front (sACCF), which corresponds to water mass boundaries as well as deep-reaching jets of eastward flow (Orsi et al., 1995). Locations of various Southern Ocean climatological fronts were obtained from the Australian Antarctic Data Centre (Orsi et al., 1995). In order to understand the circulation pattern in and around the Kerguelen Plateau, the mean dynamic topography (MDT) raster datasets (Maximenko and Niiler, 2005) were converted to contours and overlaid an Aqua-MODIS entire mission chlorophyll-*a* (Chl-*a*) composite image (2002–2013) (Fig. 1(b)). The MDT dataset was derived from combined analysis of drifters, satellite altimetry, wind, and GRACE (Gravity Recovery and Climate Experiment) satellite based geoid (www.aviso.altimetry.fr). In addition, the trajectories from ARGO float (Argo-1900046, 1901329, 1900314, 2901303, 2901306, 7900310) that crossed the entire Plateau were overlaid to illustrate the surface current patterns in and around the Plateau (Fig. 1(b)).

In-situ observations of biophysical parameters over vast portions of the southern ocean and adjoining Indian Ocean are significantly under-sampled, both temporally and spatially (Jena et al., 2013; Mishra et al., 2015). This limitation is partially overcome by the routine measurement of parameters by means of space-borne radiometers which offer synoptic and temporal sampling advantages (Moore et al., 1999; Jena et al., 2006, 2010; Kumar et al., 2012). In order to characterize the IME phenomena, Aqua-MODIS and SeaWiFS derived Chl-*a* concentration datasets based upon global standard algorithms were acquired from National Aeronautics and Space Administration (NASA) Goddard Space Flight Center (NASA's GSFC). Aqua-MODIS Level-2 data during 25th February 2013 (9:50hrs UTC, Ascending pass), was processed to generate the high spatial resolution (~1 km) Chl-*a* concentration image (Fig. 2). Level-3 climatological Chl-*a* composites from Aqua-MODIS (2002–2013) and SeaWiFS (1998–2010) were generated after discarding sea-ice and cloudy pixels. An unsupervised classification based on the ISODATA algorithm developed by Memarsadeghi et al. (2007) was performed on the Aqua-MODIS Chl-*a* composite image (2002–2013) to obtain the robust features associated with IME phenomenon around the Kerguelen Plateau (Fig. 1(b)).

Satellite datasets are known to underestimate Chl-*a* concentration at elevated *in-situ* values. For example, Moore et al. (1999) validated SeaWiFS derived Chl-*a* with *in-situ* Chl-$a_{\text{fluorescence}}$ (Chl-a_{flu}) for a range of 0.1–1.5 mg/m^3 and the results revealed that SeaWiFS underestimated the *in-situ* values. Investigations by Szeto et al. (2011) noticed that SeaWiFS Chl-*a,* using global OC4v4 algorithm, consistently underestimates Chl-*a* value by 50%, even though HPLC based measurements were considered. Earlier works defined the phytoplankton bloom as Chl-*a* concentration > 0.8 mg/m^3 (Fitch and Moore, 2007) and > 1 mg/m^3 (Moore and Abbott, 2000). After considering the underestimation tendency of satellite observations, a phytoplankton bloom is defined in this work as the pixels exceeding Chl-*a* concentration of 0.5 mg/m^3. Further, monthly composite images from Aqua-MODIS (2003–2013) and SeaWiFS (1998–2010) were used to characterize the monthly evolution of phytoplankton blooms (Chl-$a > 0.5$ mg/m^3) (Figs. 3 and 4). While estimating the areal extent of blooms, the geographic boundaries for NKP are set as 46°S to 56.5°S and 65°E to 100°E. And for SKP it is restricted from 56.5°S to coastal Antarctica and 65°E to 100°E. In this work, Austral spring-summer periods are refereed as the months of November, December, January, and February.

3 Results and discussion

Figure 1(b) indicates that wide spread low surface Chl-*a* concentration prevailed (< 0.3 mg/m^3) in the western part of the Kerguelen Plateau with the typical characteristics of HNLC water. In contrast, distinct phytoplankton blooms (Chl-$a > 0.5$ mg/m^3) observed above the Kerguelen Plateau and its downstream section along the polar front, which is attributed to IME phenomena (Figs. 1(b), 2, and 3). The presence of the Kerguelen Plateau stands as a topographic barrier to eastward ACC (Fig. 1(a)), allows a mixing process developed through turbulence and eddies which can bring subsurface iron-rich water from shallow

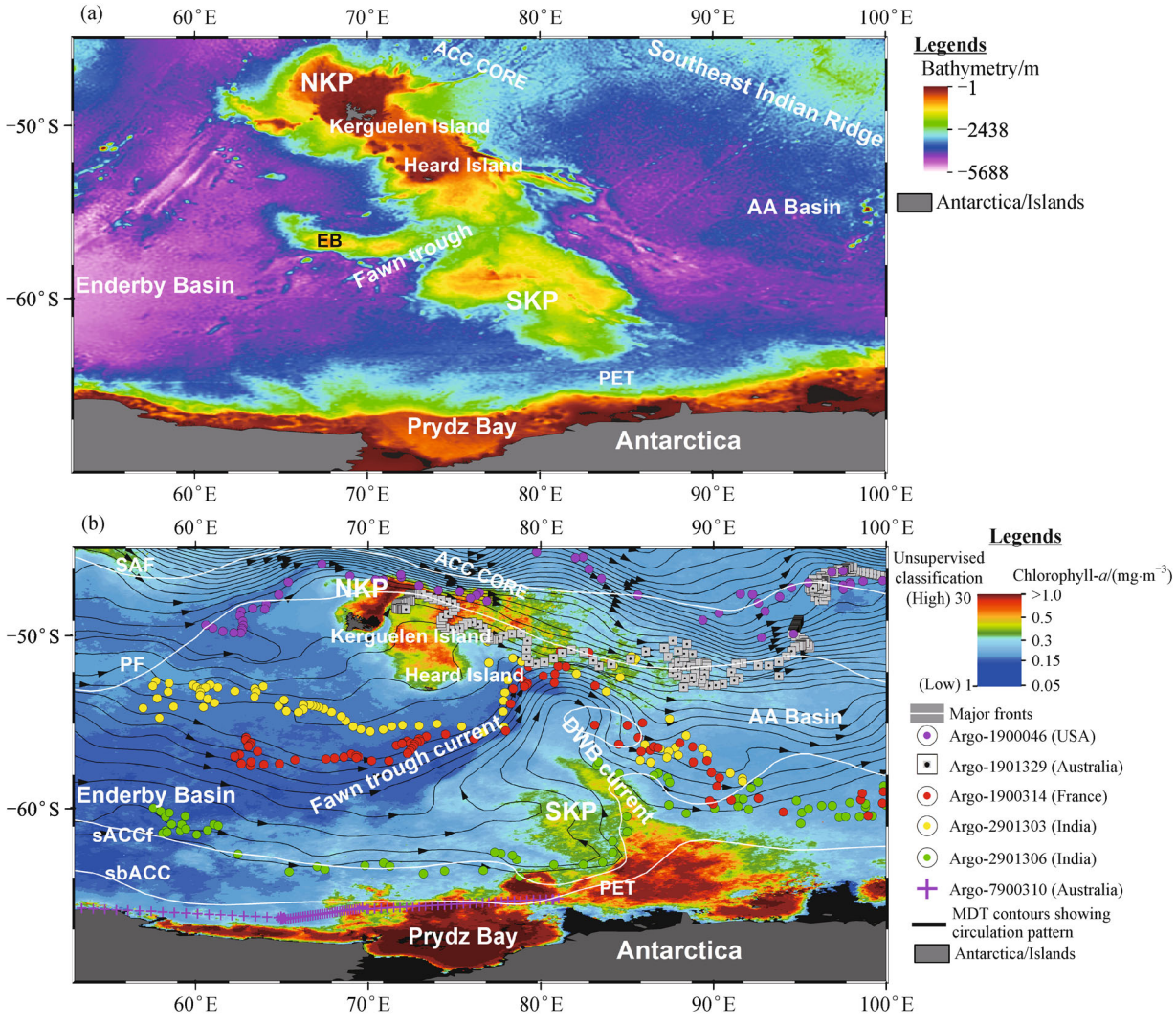

Fig. 1 (a) Map showing one arc-minute bathymetry of the Kerguelen Plateau and surrounding region, (b) An unsupervised classification based on the ISODATA algorithm is performed using Aqua-MODIS chlorophyll-*a* (Chl-*a*) composite image (2002−2013) for studying the general Chl-*a* pattern around the Kerguelen Plateau. The long-term mean dynamic topography (MDT) isolines (black solid lines) and ARGO floats (dots) were overlaid to understand the circulation pattern. The region is very dynamic after the eastward Antarctic Circumpolar Current (ACC) interacts with the Kerguelen Plateau and surrounding bathymetric features, resulting in phytoplankton blooms in the downstream section of Plateau along the polar front (PF). (SAF: Subantarctic front, sACCf: Southern Antarctic circumpolar current front, sbACC: Southern boundary of ACC, DWB: Deep western boundary current, MDT: Mean dynamic topography, AA basin: Australia-Antarctic Basin, EB: Elan Bank, PET: Port Elizabeth Trough, NKP: North Kerguelen Plateau, SKP: South Kerguelen Plateau).

Plateau to the sea surface, fertilizing the mixed layer. In addition, the interaction between high-energy internal tidal waves and bathymetry boost-up the vertical eddy diffusivity above the Kerguelen Plateau, and pumps subsurface iron to the sea surface (Park et al., 2008). An experiment carried out in October 1995 during the ANTARES 3/F-JGOFS cruise reported enrichment of dissolved iron (5.3−12.6 nmol/L) in the coastal surface waters of the Kerguelen Island and the region was associated with elevated phytoplankton biomass (Bucciarelli et al., 2001). The offshore waters were also affected by trace-metal inputs from coastal and continental shelf origin with reported dissolved iron concentrations of 0.46 to 0.71 nmol/L. Another experiment carried out for the Kerguelen Plateau and Ocean compared Study during 2004 revealed that the surface water having low iron (less than 0.09 nmol/L) on the Kerguelen Plateau was enriched by relatively high iron waters (0.19–0.51 nmol/L) emanating from a 500 m depth through a mixing process (Blain et al., 2007; Park et al., 2008). Once the mixed layer on the Plateau is fertilized, the

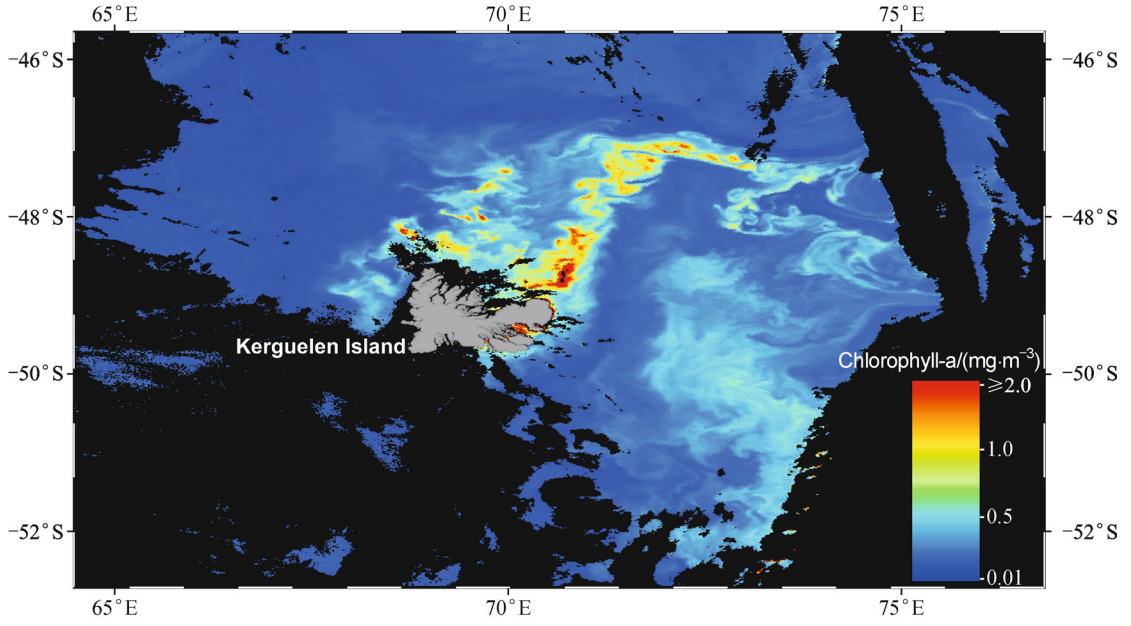

Fig. 2 High spatial resolution (~1 km) Aqua-MODIS ascending pass during 25th February 2013 (9:50 hrs UTC) showing the phytoplankton blooms off the Kerguelen Island.

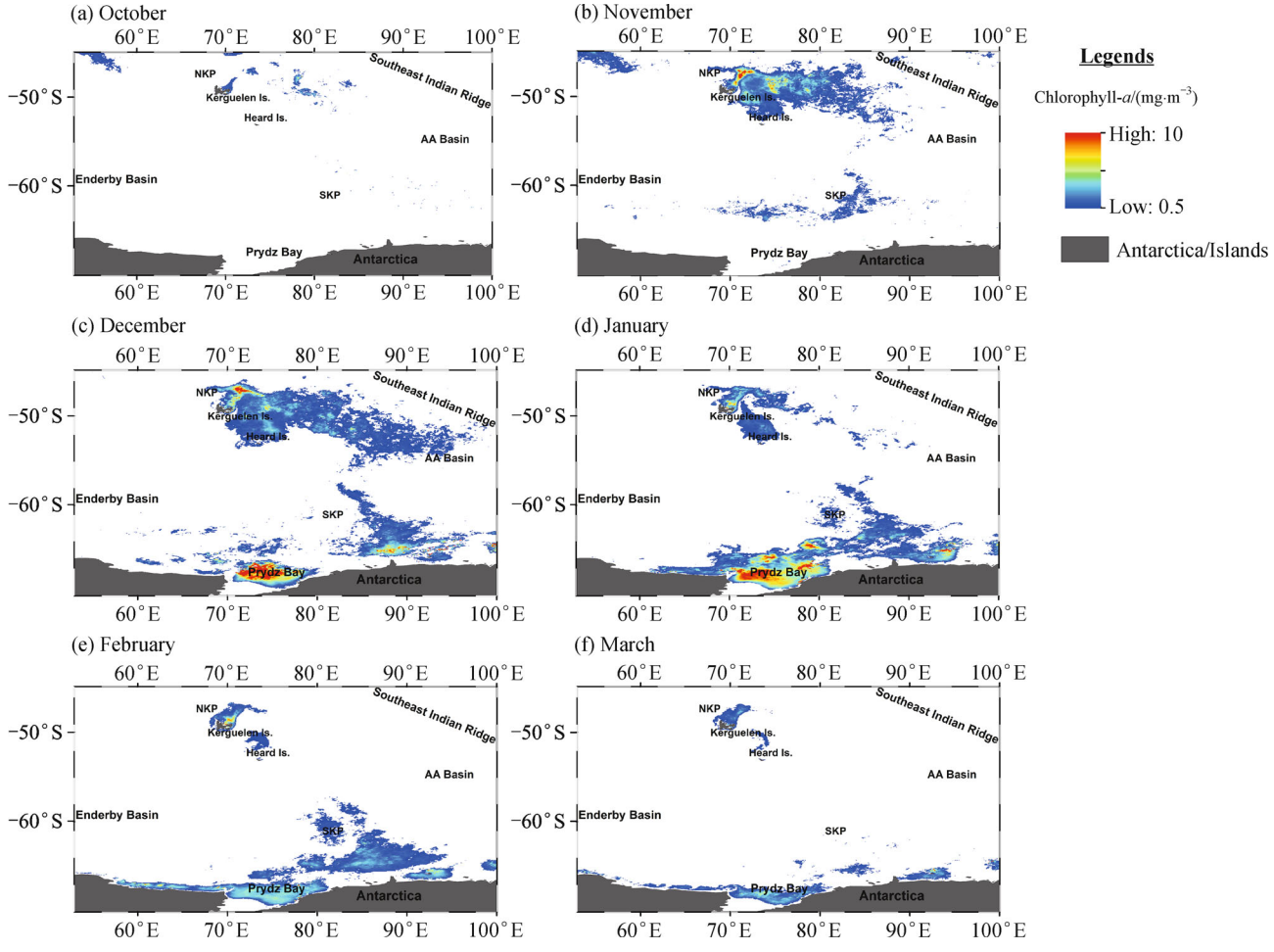

Fig. 3 Aqua-MODIS derived monthly Chl-*a* composite (2002–2013) showing the evolution of phytoplankton blooms off the Kerguelen Plateau and coastal Antarctica.

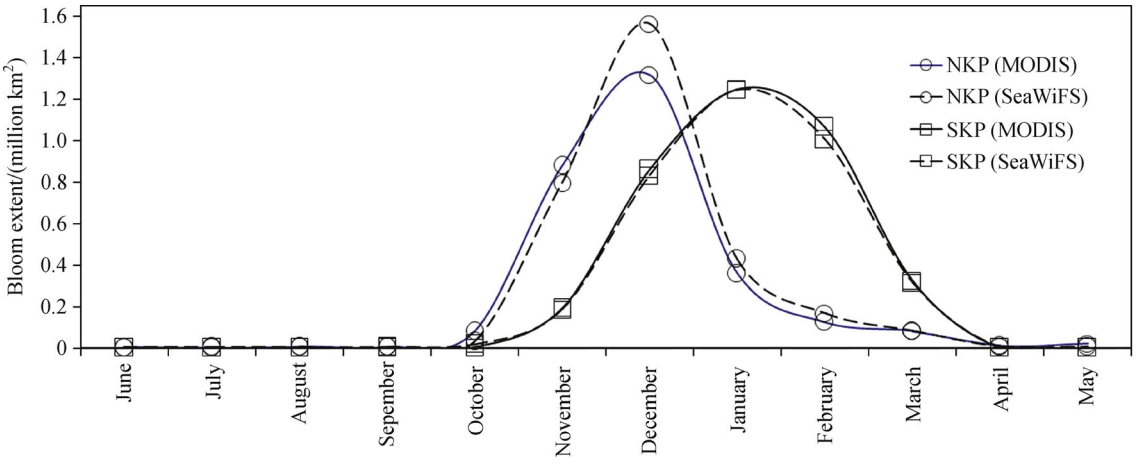

Fig. 4 Variability of monthly areal extent of phytoplankton blooms around the Kerguelen Plateau. The areal extent estimated using Aqua-MODIS monthly composite images (2002−2013) matches well with SeaWiFS (1998−2010), thus supporting the validity of observations. The northern Kerguelen Plateau (NKP) bloom peaks with a maximum areal extent of 1.315 million km^2 during December, and the southern Kerguelen Plateau (SKP) bloom peaks through a time lag of one month (January).

waters flow eastward by the persistently flowing eastward ACC. These physical processes in turn trigger enhancement of Chl-*a* concentration on the Kerguelen Plateau and its downstream sections, which provide evidence of the IME phenomena (Figs. 1(b), 2 and 3).

Earlier studies revealed wide spread low phytoplankton biomass in the Southern Ocean region, which is attributed to lack of micronutrient iron (De Baar et al., 1995; Coale et al., 1996; Gordon et al., 1997; Takeda, 1998), light limitation (Mitchell and Holm-Hansen, 1991; Nelson and Smith, 1991; Boyd et al., 2001), and strong grazing pressure (Gall et al., 2001; Selph et al., 2001; Zeldis, 2001). The artificial iron fertilization experiments revealed increase in phytoplankton biomass after addition of iron into HNLC regions (Coale et al., 1996, 2004; Boyd et al., 2000, 2007; Tsuda et al., 2003). The naturally occurring phytoplankton blooms on the Kerguelen Plateau are demonstrated in Figs. 1(b), 2 and 3, owing to IME. The light-limitation is expected to prevent phytoplankton blooms in the Southern Ocean during austral winter. Even though the light is not a limiting factor during austral summer, blooms were restricted above the Kerguelen Plateau, its downstream section, and coastal Antarctic region where enhanced iron flux to surface water is expected (Figs. 1(b) and 3).

Analysis of Aqua-MODIS and SeaWiFS monthly climatological datasets revealed that the IME phenomena is pronounced only during the austral spring-summer period, likely due to the availability of light and iron-rich water from the shallow plateau (Figs. 3 and 4). In the NKP region, the phytoplankton bloom initiates during November with an areal extent of 0.876 million km^2 and spreads to the downstream plateau section along the polar front (Figs. 3 and 4). During December, the bloom spreads further eastward as far as 1800 km offshore (up to 98°E) with an extensive areal extent of 1.315 million km^2. An offshore flow was observed with the ARGO float trajectories (Argo-1900046, 1901329) (Fig. 1(b)). The areal extent reduced considerably to 0.357 million km^2 during January (Fig. 4) and did not show its eastward existence during subsequent months except small patches near the northern part of Kerguelen Island (Fig. 3). The northwest extension of bloom along the eastern flank of SKP has in-phase correspondence with the flow pattern of deep western boundary current (DWBC) as inferred after analyzing the MDT datasets, ARGO float trajectory (Argo-2901306), and earlier reports from Donohue et al. (1999), Aoki et al. (2008) (Figs. 1(b) and 3). The flow direction of DWBC is northwestward throughout the water column emerging from the confluence of westward flow along the Antarctic continental slope and eastward flow of Weddell Basin waters through the Princess Elizabeth Trough to the south of the SKP (Donohue et al., 1999). Besides a supply of iron from the shallow plateau of SKP, the DWBC current can bring iron from the Marginal Ice Zone (MIZ) through sea-ice melting during the austral summer. Although direct deposition of iron from mineral dust is generally low in the MIZ (Luo et al., 2003; Zender et al., 2003), some dust particles from the atmosphere accumulate during winter snow fall that solidifies with the sea-ice providing a pulse input of iron during melting (Sedwick and DiTullio, 1997; Grotti et al., 2005). This mechanism can lead to bloom development at SKP. IME phenomena is apparent over SKP when the phytoplankton bloom initiates during November (0.191 million km^2) (Figs. 3 and 4). The SKP bloom peaks during January (1.245 million km^2) through

December (0.859 million km^2) and spreads eastward along the southern boundary of ACC (Figs. 3 and 4). The bloom peaks with a time lag of one month compared to the NKP bloom (Fig. 4). The SKP bloom areal extent declines during February (1.064 million km^2) and significantly loses its existence in the subsequent period. The areal extent estimated using monthly Aqua-MODIS composite image (2002−2013) matches well with SeaWiFS (1998−2010), thus supporting the validity of observations (Fig. 4). The result revealed that the Kerguelen Plateau blooms exist at least for 4 months of a year (November, December, January, and February). Even though the surface water above the Kerguelen Plateau is rich in Chl-*a*, an exception of oligotrophic condition dominated in between NKP and SKP at Fawn Trough region (Fig. 1). Sedimentary source of iron for this surface water is unlikely as the bathymetry of Fawn Trough region typically deeper than 2000 m (Fig. 1(a)). The observed oligotrophic condition could be due to apparent intrusion of iron limited low phytoplankton regime waters from the Enderby basin through the northeastward Fawn Trough Current (Fig. 1(b)). The float trajectories (Argo-1900314 and 2901303) provided evidence on the northeastward movement of the surface waters from Enderby basin to Kerguelen Plateau through Fawn Trough.

4 Conclusions

The IME phenomenon was developed after the eastward ACC encounters with the Kerguelen Plateau topography. The sedimentary source of iron from the islands and surrounding shallow plateau fertilizes the mixed layer, and possibly causes the phytoplankton bloom. Extensive blooms were observed on the Kerguelen Plateau and its downstream section for a significant period of four months in a year (November, December, January, and February). The observed physical forcing effect of biological alteration on the Kerguelen Plateau and surrounding region could draw a significant amount of CO_2 from the atmosphere, creating direct effect on the biogeochemical cycle. Satellite remote sensing datasets are well suited to observe and quantify the seasonal areal extent of phytoplankton blooms in the Kerguelen Plateau ecosystem which supports large assemblage of phytoplankton, zooplankton, seabirds, seals, and whales. Although several studies have been carried out for iron budget and carbon cycle within and outside the blooms during KEOPS cruises, the present work provided scope to study the IME phenomena using remote sensing observations.

Acknowledgements Continuous encouragement and support from the Director, National Centre for Antarctic and Ocean Research (NCAOR), and Dr. John Kurian from NCAOR are gratefully acknowledged. The institutions like the NASA's Goddard Space Flight Center and National Geophysical Data Center (NGDC) are acknowledged for making the datasets available in public domain. This is NCAOR contribution no. 05/2016.

References

Aoki S, Fujii N, Ushio S, Yoshikawa Y, Watanabe S, Mizuta G, Fukamachi Y, Wakatsuchi M (2008). Deep western boundary current and southern frontal systems of the Antarctic Circumpolar Current southeast of the Kerguelen Plateau. J Geophys Res, 113(C8): C08038

Bakker D C E, Nielsdóttir M C, Morris P J, Venables H J, Watson A J (2007). The island mass effect and biological carbon uptake for the subantarctic Crozet Archipelago. Deep Sea Res Part II Top Stud Oceanogr, 54(18−20): 2174–2190

Blain S, Quéguiner B, Armand L, Belviso S, Bombled B, Bopp L, Bowie A, Brunet C, Brussaard C, Carlotti F, Christaki U, Corbière A, Durand I, Ebersbach F, Fuda J L, Garcia N, Gerringa L, Griffiths B, Guigue C, Guillerm C, Jacquet S, Jeandel C, Laan P, Lefèvre D, Lo Monaco C, Malits A, Mosseri J, Obernosterer I, Park Y H, Picheral M, Pondaven P, Remenyi T, Sandroni V, Sarthou G, Savoye N, Scouarnec L, Souhaut M, Thuiller D, Timmermans K, Trull T, Uitz J, van Beek P, Veldhuis M, Vincent D, Viollier E, Vong L, Wagener T (2007). Effect of natural iron fertilization on carbon sequestration in the Southern Ocean. Nature, 446(7139): 1070–1074

Boyd P W, Crossley A C, DiTullio G R, Griffiths F B, Hutchins D A, Queguiner B, Sedwick P N, Trull T W (2001). Control of phytoplankton growth by iron supply and irradiance in the subantarctic Southern Ocean: experimental results from the SAZ project. J Geophys Res, 106(C12):31573–31583

Boyd P W, Jickells T, Law C S, Blain S, Boyle E A, Buesseler K O, Coale K H, Cullen J J, de Baar H J W, Follows M, Harvey M, Lancelot C, Levasseur M, Owens N P J, Pollard R, Rivkin R B, Sarmiento J, Schoemann V, Smetacek V, Takeda S, Tsuda A, Turner S, Watson A J (2007). Mesoscale iron enrichment experiments 1993–2005: synthesis and future directions. Science, 315(5812): 612–617

Boyd P W, Watson A J, Law C S, Abraham E R, Trull T, Murdoch R, Bakker D C E, Bowie A R, Buesseler K O, Chang H, Charette M, Croot P, Downing K, Frew R, Gall M, Hadfield M, Hall J, Harvey M, Jameson G, LaRoche J, Liddicoat M, Ling R, Maldonado M T, McKay R M, Nodder S, Pickmere S, Pridmore R, Rintoul S, Safi K, Sutton P, Strzepek R, Tanneberger K, Turner S, Waite A, Zeldis J (2000). A mesoscale phytoplankton bloom in the polar Southern Ocean stimulated by iron fertilization. Nature, 407(6805): 695–702

Bucciarelli E, Blain S, Tréguer P (2001). Iron and manganese in the wake of the Kerguelen Islands (Southern Ocean). Mar Chem, 73: 21–36

Caldeira R M A, Groom S, Miller P, Pilgrim D, Nezlin N P (2002). Sea-surface signatures of the island mass effect phenomena around Madeira Island, Northeast Atlantic. Remote Sens Environ, 80(2): 336–360

Coale K, Johnson K, Chavez F, Buesseler K, Barber R, Brzezinski M, Cochlan W, Millero F, Falkowski P, Bauer J, Wanninkhof R, Kudela R, Altabet M, Hales B, Takahashi T, Landry M, Bidigare R, Wang X, Chase Z, Strutton P, Friederich G, Gorbunov M, Lance V, Hilting A, Hiscock M, Demarest M, Hiscock W, Sullivan K, Tanner S, Gordon R, Hunter C, Elrod V, Fitzwater S, Jones J, Tozzi S, Koblizek M, Roberts A, Herndon J, Brewster J, Ladizinsky N, Smith G, Cooper D, Timothy D, Brown S, Selph K, Sheridan C, Twining B, Johnson Z (2004). Southern Ocean Iron Enrichment Experiment (SOFeX): carbon cycling in high- and low-Si waters. Science, 304(5669): 408–

414

Coale K H, Johnson K S, Fitzwater S E, Gordon R M, Tanner S, Chavez F P, Ferioli L, Sakamoto C, Rogers P, Millero F, Steinberg P, Nightingale P, Cooper D, Cochlan W P, Landry M R, Constantinou J, Rollwagen G, Trasvina A, Kudela R (1996). A massive phytoplankton bloom induced by an ecosystem-scale iron fertilization experiment in the equatorial Pacific Ocean. Nature, 383(6600): 495–501

De Baar H J W, de Jong J T M, Bakker D C E, Loscher B M, Veth C, Bathmann U, Smetacek V (1995). Importance of iron for plankton blooms and carbon dioxide drawdown in the Southern Ocean. Nature, 373(6513): 412–415

Donohue K A, Hufford G E, McCartney M S (1999). Sources and transport of the deep western boundary current east of the Kerguelen Plateau. Geophys Res Lett, 26(7): 851–854

Doty M S, Oguri M (1956). The island mass effect. Journal of the International Council for the Exploration of the Sea, 22: 33–37

Fitch D T, Moore J K (2007). Wind speed influence on phytoplankton bloom dynamics in the Southern Ocean Marginal Ice Zone. J Geophys Res, 112(C8): C08006

Gall M P, Boyd P W, Hall J, Safi K A, Chang H (2001). Phytoplankton processes: Part I. community structure during the Southern Ocean Iron Release Experiment (SOIREE). Deep Sea Res Part II Top Stud Oceanogr, 48(11−12): 2551–2570

Gordon R M, Coale K H, Johnson K S (1997). Iron distributions in the equatorial Pacific: implications for new production. Limnol Oceanogr, 42(3): 419–431

Grotti M, Soggia F, Ianni C, Frache R (2005). Trace metals distributions in coastal sea ice of Terra Nova Bay, Ross Sea, Antarctica. Antarct Sci, 17(2): 289–300

Heywood K J, Barton E D, Simpson J H (1990). The effects of flow disturbance by an oceanic island. J Mar Res, 48(1): 55–73

Heywood K J, Stevens D P, Bigg G R (1996). Eddy formation behind the tropical island of Aldabra. Deep Sea Res Part I Oceanogr Res Pap, 43 (4): 555–578

Jena B, Kurian P J, Swain D, Tyagi A, Ravindra R (2012). Prediction of bathymetry from satellite altimeter based gravity in the Arabian Sea: mapping of two unnamed deep seamounts. Int J Appl Earth Obs Geoinf, 16: 1–4

Jena B, Rao M V, Sahu B K (2006). TRMM derived sea surface temperature in the wake of a cyclonic storm over the central Bay of Bengal. Int J Remote Sens, 27(14): 3065–3072

Jena B, Sahu S, Kumar A, Swain D (2013). Observation of oligotrophic gyre variability in the south Indian Ocean: environmental forcing and biological response. Deep Sea Res Part I Oceangr Res Pap, 80: 1–10

Jena B, Swain D, Tyagi A (2010). Application of artificial neural networks for sea-surface wind-speed retrieval from IRS-P4 (MSMR) brightness temperature. IEEE Geosci Remote S, 7(3): 567–571

Kumar A, Jena B, Vinaya M S, Jayappa K S, Narayana A C, Bhat H G (2012). Regionally tuned algorithm to study the seasonal variation of suspended sediment concentration using IRS-P4 Ocean Colour Monitor data. Egyp J Remote Sens Space Sci, 15 (1): 67–81

Luo C, Mahowald N M, Del Corral J (2003). Sensitivity study of meteorological parameters on mineral aerosol mobilization, transport and distribution. J Geophys Res, 108(D15): 4447

Martin J H, Gordon R M, Fitzwater S E (1990). Iron in Antarctic waters. Nature, 345(6271): 156–158

Maximenko N A, Niiler P P (2005). Hybrid decade-mean global sea level with mesoscale resolution. In: Saxena, N, ed. Recent Advances in Marine Science and Technology 2004. PACON International: 55–59

Memarsadeghi N, Mount D M, Netanyahu N S, Le Moigne J (2007). A fast implementation of the ISODATA clustering algorithm. Int J Comput Geom Appl, 17(1): 71–103

Minas H J, Minas M (1992). Net community production in high nutrient-low chlorophyll waters of the tropical and Antarctic Oceans: grazing vs. iron hypothesis. Oceanol Acta, 15: 145–162

Mishra R K, Naik R K, Anilkumar N (2015). Adaptations of phytoplankton in the Indian Ocean sector of the Southern Ocean during austral summer of 1998–2014. Front Earth Sci, 9(4): 742–752

Mitchell B G, Holm-Hansen O (1991). Bio-optical properties of Antarctic Peninsula waters: differentiation from temperate ocean models. Deep Sea Res Part I Oceanogr Res Pap, 38(8–9): 1009–1028

Moore J K, Abbott M R (2000). Phytoplankton chlorophyll distributions and primary production in the Southern Ocean. J Geophys Res, 105 (C12): 28709–28722

Moore J K, Abbott M R, Richman J G, Smith W O, Cowles T J, Coale K H, Gardner W D, Barber R T (1999). SeaWiFS satellite ocean color data from the Southern Ocean. Geophys Res Lett, 26(10): 1465–1468

Nelson D M, Smith W O (1991). Sverdrup revisited: critical depths, maximum chlorophyll levels, and the control of Southern Ocean productivity by the irradiance-mixing regime. Limnol Oceanogr, 36 (8): 1650–1661

Orsi A H, Whitworth T III, Nowlin W D Jr (1995). On the meridional extent and fronts of the Antarctic Circumpolar Current. Deep Sea Res Part I Oceanogr Res Pap, 42(5): 641–673

Palacios D M (2002). Factors influencing the island-mass effect of the Galápagos Archipelago. Geophys Res Lett, 29(23): 49-1–49-4

Park Y H, Fuda J L, Durand I, Naveira Garabato A C (2008). Internal tides and vertical mixing over the Kerguelen Plateau. Deep Sea Res Part II Top Stud Oceanogr, 55(5−7): 582–593

Sedwick P N, DiTullio G R (1997). Regulation of algal blooms in Antarctic shelf water by the release of iron from melting sea ice. Geophys Res Lett, 24(20): 2515–2518

Selph K E, Landry M R, Allen C B, Calbet A, Christensen S, Bidigare R R (2001). Microbial community composition and growth dynamics in the Antarctic Polar Front and seasonal ice zone during late spring 1997. Deep Sea Res Part II Top Stud Oceanogr, 48(19−20): 4059–4080

Signorini S R, McClain C R, Dandonneau Y (1999). Mixing and phytoplankton bloom in the wake of the Marquesas Islands. Geophys Res Lett, 26(20): 3121–3124

Sunda W G (1989). Trace metal interactions with marine phytoplankton. Biol Oceanogr, 6: 411–442

Szeto M, Werdell P J, Moore T S, Campbell J W (2011). Are the worlds oceans optically different? Journal of Geophysical Research, 116 (C00H04), doi:10.1029/2011JC007230

Takeda S (1998). Influence of iron availability on nutrient consumption ratio of diatoms in oceanic waters. Nature, 393(6687): 774–777

Tsuda A, Takeda S, Saito H,Nishioka J, Nojiri Y, Kudo I, Kiyosawa H, Shiomoto A, Imai K,Ono T, Shimamoto A, Tsumune D, Yoshimura T, Aono T,Hinuma A, Kinugasa M, Suzuki K, Sohrin Y, Noiri Y, Tani H, Deguchi Y, Tsurushima N, Ogawa H, Fukami K, Kuma K,

Saino T (2003). A mesoscale iron enrichment in the western subarctic Pacific induces a large centric diatom bloom. Science, 300 (5621): 958–961

Venables H J, Moore C M (2010). Phytoplankton and light limitation in the Southern Ocean: learning from high nutrient high chlorophyll areas. J Geophys Res, 115(C2 C02015): C02015

Zeldis J (2001). Mesozooplankton community composition, feeding, and export production during SOIREE. Deep Sea Res Part II Top Stud Oceanogr, 48(11−12): 2615–2634

Zender C S, Bian H, Newman D (2003). Mineral Dust Entrainment and Depositon (DEAD) model: description and 1990s dust climatology. J Geophys Res, 108(D14): 4416